Detecting beta-amyloid aggregation from the time-resolved emission spectra.

A.Alghamdi[1], V.Vyshemirsky[2], D.J.S.Birch[1,3], O.J.Rolinski[1]

[1]Photophysics Group, Centre for Molecular Nanometrology, Department of Physics, Scottish Universities Physics Alliance, University of Strathclyde, 107 Rottenrow, Glasgow G4 0NG, UK.

[2]School of Mathematics and Statistics, University of Glasgow, Glasgow G12 8QQ, UK.

[3]HORIBA Jobin Yvon IBH Ltd, 133 Finnieston Street, Glasgow G3 8HB, UK.

E-mail: o.j.rolinski@strath.ac.uk

Abstract

Aggregation of beta-amyloids is one of key processes responsible for the development of Alzheimer's desease. Early molecular-level detection of beta-amyloid oligomers may help in early diagnosis and in the development of new intervention therapies. Our previous studies on changes in beta-amyloid's single tyrosine intrinsic fluorescence response during aggregation demonstrated a four-exponential fluorescence intensity decay, and that the ratio of the pre-exponential factors indicated the extent of aggregation in the early stages of the process before the beta-sheets are formed. Here we present a complementary approach based on time-resolved emission spectra (TRES) of amyloid's tyrosine excited at 279 nm and fluorescent in the window 240-450 nm. TRES has been used to demonstrate sturctural changes occuring on the nanosecond time scale after excitation which has significant advantages over using steady-state spectra. We demonstrate this by resolving the fluorescent species and revealing that beta-amyloid's monomers show very fast dielectric relaxation and its oligomers display a substantial spectral shift due to dielectric relaxation, which gradually decreases when oligomers become larger

1. Introduction

Beta-amyloids (Aβs) are fragments of an integral membrane Amyloid precursor protein (APP). The enzymatic processes responsible for the metabolism of APP to Aβ are now reasonably well understood[1]. However, the role of Aβs in normal physiology remains unclear. Aβs are found in nanomolar concentrations in biological fluids[2]. At these low concentrations Aβs remain monomeric and function as antioxidants[3]. At the higher concentrations Aβs start aggregating[4,5]– initially into small permeable oligomers that travel freely into the brain, and, in the later stages, into plaques that are hallmarks of Alzheimer's disease[6]. Many studies[7,8] demonstrated that Alzheimer's disease may begin at the molecular level long before the development of plaques because small oligomers of Aβ strongly interfere with the neuron function. Therefore, detecting oligomerization of Aβ at its early stages in terms of understanding how aggregation begins, how the local environment affects the aggregation pathway and what can be done to inhibit this aggregation before soluble toxic oligomers are formed is paramount for developing intervention therapies.

A significant research effort has been done in recent years to reveal detailed molecular mechanisms of oligomerisation and fibrillisation of amyloids. The common approach used to detect aggregation involves labelling Aβ with the dyes sensitive to the formation of beta sheets like thioflavin T (ThT)[9-11] or undergoing intramolecular interactions like TAMRA.[12] In these cases the changes in the label's fluorescence (intensity or decay) were used as the indicators of amyloid aggregation. Several attempts employing the fluorescence correlation spectroscopy and labelling the amyloids with the fluorescent probes like ARCAM-1[13], ThT[14] or HiLyte Fluor 488[15] allowed characterisation of aggregation intermediates during the assembly process. The other techniques, like the cross-correlation spectroscopy at the single-molecule fluorescence level [16] were used to investigate the impact of other proteins on inhibiting amyloid aggregation.

Majority of the techniques used for investigating beta-amyloid performance on molecular level use the Aβ labelled dyes. Our approach to this task is to use the sub-ns time and sub-nm spatial resolution of the time-resolved fluorescence spectroscopy of intrinsic fluorophores. This allows a non-invasive detection of very small changes in the surroundings of the fluorophore without disturbing its native structure. For example, we have demonstrated[17] that when exciting Aβ with a 279 nm pulsed LED source Aβ's single tyrosine (Tyr) fluorescence decay responds to the changes in its environment induced by peptide oligomerization from the early stages. Unfortunately the intrinsic fluorescence decay of amino acids such as Tyr in solution is complicated and has remained unresolved over several decades. Typically, such decays are analysed by fitting to multi-exponential functions which are explained by one of two contradictory views of the excited state processes: the rotamer model (assuming discrete ground-state conformations[18,19]) and the dielectric relaxation model (spectral shift due to dipolar relaxation[20,21]). Our previous beta-amyloid studies[17,22,23] , based on Tyr fluorescence and molecular dynamics simulations, suggested that the Tyr fluorescence decay can be adequately explained by a four-rotamer model. Moreover, the plot of the ratio of pre-exponential factors vs. time can serve as a calibration curve for determining the extent of Aβ oligomerisation. More recently we have shown the alternative model with less variables, which also fits well to the Aβ decay during oligomerisation, and assumes a continuous stable distribution of the fluorescence transition rates resulting in the non-Debye fluorescence intensity decay function[24]

$$I_{\alpha,\kappa}(t) = exp\left[-\frac{1}{\kappa}\int_0^{\kappa\left(\frac{t}{\tau_o}\right)^{\alpha}}\left(1-exp\left[-\frac{1}{x}\right]\right)dx\right] \quad (1)$$

where τ_o (of the dimension of time) and the non-dimensional parameters α and κ determine the stable distributions of fluorescence transition rates. Tracking the evolution of τ_o, α and κ during Aβ aggregation has shown[25] that α takes values larger than 1 during the first 40 hours of aggregation, which is not possible if the relaxation of the excited-states is the only process occurring, no matter what is the distribution of the transition rates . This observation led us to the conclusion that the experimental decay may be determined by the decay of the excited population while being interfered with by the dielectric relaxation.

In this paper we present the evidence that the dielectric relaxation affects the fluorescence decays of Tyr in Aβ and investigate the suitability of this process as an indicator of the stage of aggregation. In our approach, we assume that both the dielectric relaxation and depopulation of the excited states occur at the same time scale and thus both affect the fluorescence decay. Previous research[26,27] suggests that these processes can be distinguished from each other by a quantitative model of simultaneous decay and electrostatic relaxation. Note that this model assumes the existence of a single form of a fluorophore, where the transient spectra decreases its intensity and shifts towards lower energies, but maintains its shape. Here we investigate whether the aggregating amyloids can be described by a similar model, or consideration of more than one fluorescent residue is needed. For this purpose we monitor the TRES changes in Aβ sample during its aggregation over 8 days.

2. Experimental

The data reported here were obtained for a 50 μM sample of $A\beta_{(1-40)}$ (Sigma-Aldrich) in HEPES buffer of pH7.4. It is important to note that a freshly prepared sample may not be composed of the $A\beta_{(1-40)}$ monomers only and some contribution of small oligomers may be expected and this has been also confirmed in these studies. The sample was incubated at the temperature of 36^{o}C over the whole period of experiment. The amyloid suspension was kept in a micro-cuvette of the volume of ~140 μL and was not stirred during the experiment.

Steady-state fluorescence spectra measurements of $A\beta_{(1-40)}$ were obtained using the Fluorolog-3 Spectrofluorometer. The excitation settings were 279 nm with a slit width of 5 nm and the fluorescence was detected at the emission window of 290-450 nm in increments of 1 nm with a slit width 5nm.

Time Correlated Single Photon Counting (TCSPC) measurements were conducted on a Horiba Scientific DeltaFlex Hybrid fluorometer (Horiba Jobin Yvon IBH Ltd, Glasgow, UK). The excitation source used was a Horiba NanoLED with excitation at 279 nm, pulse duration 50 ps and repetition rate of 1MHz.

For every measurement, 12 decay curves were collected at the emission wavelengths between 294 and 327 nm at 3 nm increments. The obtained decay curves were then analysed by a deconvolution program that assumes a 3-exponential decay of fluorescence and accounts for the presence of scattered excitation light in the Tyr decay (see Fig. 1a). Adding more components to the decay model showed no further improvements to the fit. For example, the fourth component in the 4-exponential model usually appeared with the negative amplitude and the lifetime almost identical to one of the other three lifetimes, which supports the 3-exponential model. The fluorescence decays $f_\lambda(t)$ measured at different detection wavelengths λ were then used to calculate the TRES $I_t(\lambda)$ according to the equation

$$I_t(\lambda) = f_\lambda(t) \times \frac{S(\lambda)}{\int_0^\infty I_\lambda(t)dt} \qquad (2)$$

where S(λ) is the steady-state fluorescence spectrum, and the integral is proportional to the total emitted photons in the lifetime experiment. The obtained spectra were then converted from the wavelength $I_t(\lambda)$ to the wavenumber scale according to $I_t(\nu) = \lambda^2 I_t(\lambda)$.

The evolution of spectral centroid $\nu_c(t)$ defined as

$$\nu_c(t) = \frac{\nu_1(t)A_1(t)+\nu_2(t)A_2(t)}{A_1(t)+A_2(t)} \qquad (3)$$

was also used in the data analysis.

3. Results and discussion

Experimental observations of Aβ's fluorescence intensity decays (Fig.1b) show that the mean decay lifetime increases with the increase of the detection wavelength, which is consistent with the lifetime-wavelength correlation usually observed in protein fluorescence. We can also see that the decays evolve when the sample ages. For example, the fluorescence decays at detection wavelength 297 nm show that the mean lifetime at the Day 8 is shorter than at the Day 1, whereas decays at the detection wavelength 327 nm have a similar mean lifetime. Fitting the decays to the three-exponential model (Fig.1a), shows that at early stage of aggregation (Day1) all three lifetimes increase with the detection wavelength. At the late stage of aggregation (Day 8), the increase in lifetimes is smaller and the lifetime-wavelength correlation can hardly be observed. The contributions of scattered light (parameter C in Fig.1a) show that decay curves measured at short detection wavelengths are highly affected by scattered excitation light, especially at the late stages of aggregation. For example, the contribution of scattered light at the detection wavelength 297 nm is 10.6 % at the Day 1 and increases to 21.5 % at the Day 8.

The TRES $I_t(\nu)$ were calculated for several fixed times. Fig.1c shows the examples of 6 spectra at different times after excitation measured on Day 1 and then on Day 8. In the next stage we have modelled $I_t(\nu)$ using the Toptygin-type approach[26] where the sum of two normalised Gaussian profiles were used to represent the shape of the emission spectra

$$I_t(\nu) = \nu^3 \left(\frac{A_1(t)}{\sqrt{2\pi\sigma_1^2(t)}} \exp\left[\frac{-(\nu-\nu_1(t))^2}{2\sigma_1^2(t)}\right] + \frac{A_2(t)}{\sqrt{2\pi\sigma_2^2(t)}} \exp\left[\frac{-(\nu-\nu_1(t))^2}{2\sigma_2^2(t)}\right] \right). \qquad (4)$$

Here t is time after excitation in ns, ν is wavenumber in cm^{-1}, $A_1(t)$ and $A_2(t)$ are the amplitudes of each component, while $\sigma_1(t)$ and $\sigma_2(t)$ are the standard deviations and the $\nu_1(t)$ and $\nu_2(t)$ are their peaks positions.

The observed good fit of the function from Eqtn.4 to the experimental TRES data may be an indication of the existence of two fluorescent forms, but we cannot exclude that there is a single form with a double-peak spectrum. If the latter is the case the spectrum should shift as a whole monotonically towards shorter wavenumbers. To investigate this option we have inspected the changes in the position of the spectral centroid $\nu_c(t)$.

A plot of $\nu_c(t)$ against time t is shown in Fig.1d. The change in spectral centroid ν_c (t) is non-exponential. In fact, an initial increase is observed before a gradual decrease occurs. This non-monotonic behaviour of $\nu_c(t)$ suggest a more complex composition of the sample and has brought us to the hypothesis, that the sample contains two or more different forms both involved in the solute solvent-relaxation with the peaks undergoing the exponential decays at their own rates. The parameters obtained from fitting the 2-Gaussian profile to the TRES are plotted in the Fig. 2a, b and c.

The parameters describing the position of each peak $\nu_1(t)$ starting at 33000 cm^{-1} and $\nu_2(t)$ starting at 30500 cm^{-1} evolve in time as shown in Fig.2a. The position of the first peak $\nu_1(t)$ does not show significant changes in time indicating slow dielectric relaxation. Currently we associate this peak with Aβ monomers. Monomers are expected to have a short dielectric relaxation time due to their small size and concomitant tyrosine's exposure to water, thus the dielectric relaxation process is almost completed before the fluorescence occurs and therefore has a very weak effect on the shift of fluorescence peak.

The position of the second peak $\nu_2(t)$ shifts exponentially from an initial value $\nu_2(0)$ to a substantially lower energy value $\nu_2(\infty)$ with the relaxation time $\tau_r \approx 8$ ns. The dielectric relaxation times τ_r of the second form (see Table 1) increase as the sample ages, suggesting the gradual growth of the formed oligomers. This relaxation time can be therefore used as an indicator of the progress of Aβ aggregation. Oligomerisation explains the initial shift of the emission peak from 33000 cm^{-1} to about 30500 cm^{-1} and its further red shift due to dielectric relaxation.

Fig.2b shows that the standard deviation of the first peak $\sigma_1(t)$ doesn't change significantly, as the sample ages, because Aβ s are still in monomeric form. On the contrary, the standard deviation of the second peak $\sigma_2(t)$ becomes narrower at later times. Our interpretation of this observation is that at early stages of aggregation the oligomers are small and have freedom to rotate thus the variety of tyrosine surroundings is relatively broad, which results in large spread of solvation energies and consequently broader spectrum. As the sample ages aggregates become larger the surroundings of the tyrosines become more uniform and the rotational freedom limited.

Because the Gaussian functions used in the equation (4) are normalised, the parameters A_1 and A_2 can be considered as the fluorescence contributions of each component. Thus, the plots of A_1 and A_2 vs. time (Fig. 2c) represent the decays of fluorescence intensity of each component individually. The results show that the mean lifetime of the second peak is highly affected by Aβ aggregation suggesting that, at the early stages of aggregation, the impact of dielectric relaxation on the fluorescence decay curve is strong. The first peak doesn't show any significant changes in the mean lifetime, which is consistent with the first peak representing monomers.

The ratio $A_1(0)/A_2(0)$ shows that the contribution of the monomer peak is dominant but slightly decreases as the sample ages (Fig. 2d). The $A_1(t)/A_2(t)$ ratio changes after excitation as shown in Fig. 2e, which is a result of two components decaying at different rates. In the course of aggregation, the ratio $A_1(t)/A_2(t)$ evolves differently on the nanosecond scale due to the change in the amount and mean decay time of oligomers, and therefore can be used as an indication of the stage of aggregation.

4. Conclusion

Changes in the time resolved emission spectra of the aggregating beta-amyloids indicate at least two different sub-systems of fluorescent tyrosine; one originating from Tyr in monomers and the other from Tyr in oligomers. The latter decay is highly influenced by the dielectric relaxation process, which can be used to determine the extent of aggregation.

The observed kinetics is complex and the multi-exponential functions need to be fitted to the experimental decays to satisfy the goodness of fit criteria. The multi-exponential approach is sufficient for determining TRES from the raw fluorescence decays. However, because we demonstrated that the dielectric relaxation substantially impacts the observed decays, this process cannot be neglected in the proper model of the kinetics. Therefore, in the studies of protein aggregation the kinetic models combining both the dielectric relaxation and the specific mechanism of depopulation of the excited states (e.g. one governed by the stable distribution of the decay rates[27]) should be considered to represent properly the fluorescence characteristics of the heterogenic molecular system.

5. Acknowledgements

The authors have declared that no conflicting interests exist.

A. A. wishes to thank PNU for financial support.

References:

1. Selkoe, D. J. Alzheimer ' s Disease : Genes , Proteins , and Therapy. Physiol. Rev. **81,** 741–766 (2001).

2. Seubert, P. et al. Isolation and quantification of soluble Alzheimer's beta-peptide from biological fluids. Nature **359,** 325–327 (1992).

3. Kontush, A. Amyloid-B : An antioxidant that becomes a pro-oxidant and critically contributes to Alzheimer's disease. Free Radic. Biol. Med. **31,** 1120–1131 (2001).

4. Harper, J. D., Wong, S. S., Lieber, C. M. & Lansbury, P. T. Assembly of A Amyloid Protofibrils : An in Vitro Model for a Possible Early Event in Alzheimer ' s Disease . Biochemistry **38,** 8972–8980 (1999).

5. Lomakin, A., Teplow, D. B., Kirschner, D. A. & Benedek, G. B. Kinetic theory of fibrillogenesis of amyloid β-protein. Proc. Natl. Acad. Sci. **94,** 7942–7947 (1997).

6. Hardy, J. & Selkoe, D. J. The Amyloid Hypothesis of Alzheimer ' s Disease : Progress and Problems on the Road to Therapeutics. Science (80-.). **297,** 353–356 (2002).

7. Kim, T., Vidal, G.S., Djurisic, M., William, C.M., Birnbaum, M.E., Garcia, K.C., Hyman, B.T. and Shatz, C. J. Science **341,** 1399–1404 (2013).

8. Murphy, M. P. & Levine III, H. Alzheimer`s Disease and the β-Amyloid Peptide. *J. Alzheimer's Dis.* **19,** 1–17

(2010).

9. Batzli, K. M. and Love, B. J. Materials Science and Engineering: C, **48**, 359-364 (2015).

10. Guo, J., Yu, L., Sun, Y. and Dong, X. The Journal of Physical Chemistry B, **121**(16), 3909-3917 (2017).

11. Wang, Y., Clark, T. B., and Goodson III, T. The Journal of Physical Chemistry B, **114**(20), 7112-7120 (2010).

12. Girych, M., Gorbenko, G., Maliyov, I., Trusova, V., Mizuguchi, C., Saito, H., and Kinnunen, P. Methods Appl. Fluoresc. 4(3), 034010 (2016).

13. Guan, Y., Cao, K. J., Cantlon, A., Elbel, K., Theodorakis, E. A., Walsh, D. M. and Shah, J. V. ACS chemical neuroscience, **6**(9), 1503-1508 (2015).

14. Tiiman, A., Jarvet, J., Gräslund, A. and Vukojević, V. Biochemistry, **54**(49), 7203-7211. (2015).

15. Nandi, S., Mondal, P., Chowdhury, R., Saha, A., Ghosh, S. and Bhattacharyya, K. Physical Chemistry Chemical Physics, **18**(44), 30444-30451 (2016).

16. Zheng, Y., Tian, S., Peng, X., Yang, J., Fu, Y., Jiao, Y. and Hong, T. FEBS Letters, **590**(7), 1028-1037 (2016).

17. Rolinski, O. J., Amaro, M. & Birch, D. J. S. Biosensors and Bioelectronics Early detection of amyloid aggregation using intrinsic fluorescence. Biosens. Bioelectron. **25,** 2249–2252 (2010).

18. Szabo, A. G. & Rayner, D. M. Fluorescence Decay of Tryptophan Conformers in aqueous solution. J. Am. Chem. Soc. **102,** 554–563 (1980).

19. Dahms, T. E. S., Willis, K. J. & Szabo, A. G. Conformational Heterogeneity of Tryptophan in a Protein Crystal. J. Am. Chem. Soc. **117,** 2321–2326 (1995).

20. Lakowicz, J. R. Principles of Fluorescence Spectroscopy, 3rd edition, Springer (2006).

21. Lakowicz, J. R. Invited Review On Spectral Relaxation in Proteins. Photochem. Photobiol. **72,** 421–437 (2000).

22. Amaro, M., Kubiak-Ossowska, K., Birch, D. J. S. & Rolinski, O. J. Initial stages of beta-amyloid A β 1 − 40 and A β 1 − 42 oligomerization observed using fluorescence decay and molecular dynamics analyses of tyrosine. Methods Appl. Fluoresc. **1,** 15006 (2013).

23. Amaro, M. et al. Inhibition of beta-amyloid aggregation by fluorescent dye labels Inhibition of beta-amyloid aggregation by fluorescent dye labels. Appl. Phys. Lett. **104,** 63704 (2014).

24. Rolinski, O. J. & Vyshemirsky, V. Fluorescence kinetics of tryptophan in a heterogeneous environment. Methods Appl. Fluoresc. **2,** 45002 (2014).

25. Rolinski, O. J., Wellbrock, T., Birch, D. J. S. & Vyshemirsky, V. Tyrosine Photophysics during the Early Stages of B-Amyloid Aggregation Leading to Alzheimer's. J. Phys. Chem. Lett. **6,** 3116–3120 (2015).

26. Toptygin, D. & Brand, L. Spectrally-and time-resolved fluorescence emission of indole during solvent relaxation: a quantitative model. Chem. Phys. Lett. **322,** 496–502 (2000).

27. Rolinski, O. J., McLaughlin, D., Birch, D. J. S. & Vyshemirsky, V. Resolving environmental microheterogeneity and dielectric relaxation in fluorescence kinetics of protein. Methods Appl. Fluoresc. **4,** 24001 (2016).

Table 1. The TRES second peak's positions $\nu_2(0)$ and $\nu_2(\infty)$, and the dielectric relaxation times τ_r. The average error in the peak positions is ±40 cm^{-1} and in the relaxation times is ±0.9 ns.

	1 hr	**5 hrs**	**24 hrs**	**48 hrs**	**72 hrs**	**96 hrs**	**168 hrs**
$\nu_2(0)/cm^{-1}$	30410	30369	30374	30377	30329	30314	30323
$\nu_2(\infty)/cm^{-1}$	29007	29032	29942	29915	30146	30169	30205
τ_r/ns	6.6	8.4	8.5	8.9	9.0	10.6	10.9

Figure Captions:

Figure 1. a) Fluorescence decay data of beta-amyloid at the detection wavelengths 297 and 327 nm together with the excitation pulse, fitted 3-exponential function, the scattered light term (C) and the distribution of residuals. b) The time-wavelength correlation observed in two decays of beta-amyloid at detection wavelengths 297 and 327 nm and at two different stages of aggregation: Day 1 and Day 8. The insets show the peak areas of the experimental curves. c) Time resolved emission spectra (TRES) obtained at two different stages of aggregation (Day 1 and Day 8) fitted to a two Gaussian profile. d) The change in the centroid of the emission spectrum (see Eqtn (3)) on the nanosecond scale at different stages of aggregation.

Figure 2. a) Evolution of the peak positions $\nu_1(t)$ and $\nu_2(t)$. b) Standard deviation of both peaks $\sigma_1(t)$ and $\sigma_2(t)$ at different stages of aggregation. c) Fluorescence intensity decay of each component (monomers A_1, oligomers A_2). d) The initial percentage contribution of each component $A_1(0)/A_2(0)$ at the different stages of aggregation. e) The ratio of the monomer to oligomer contribution $A_1(t)/A_2(t)$ plotted against time.

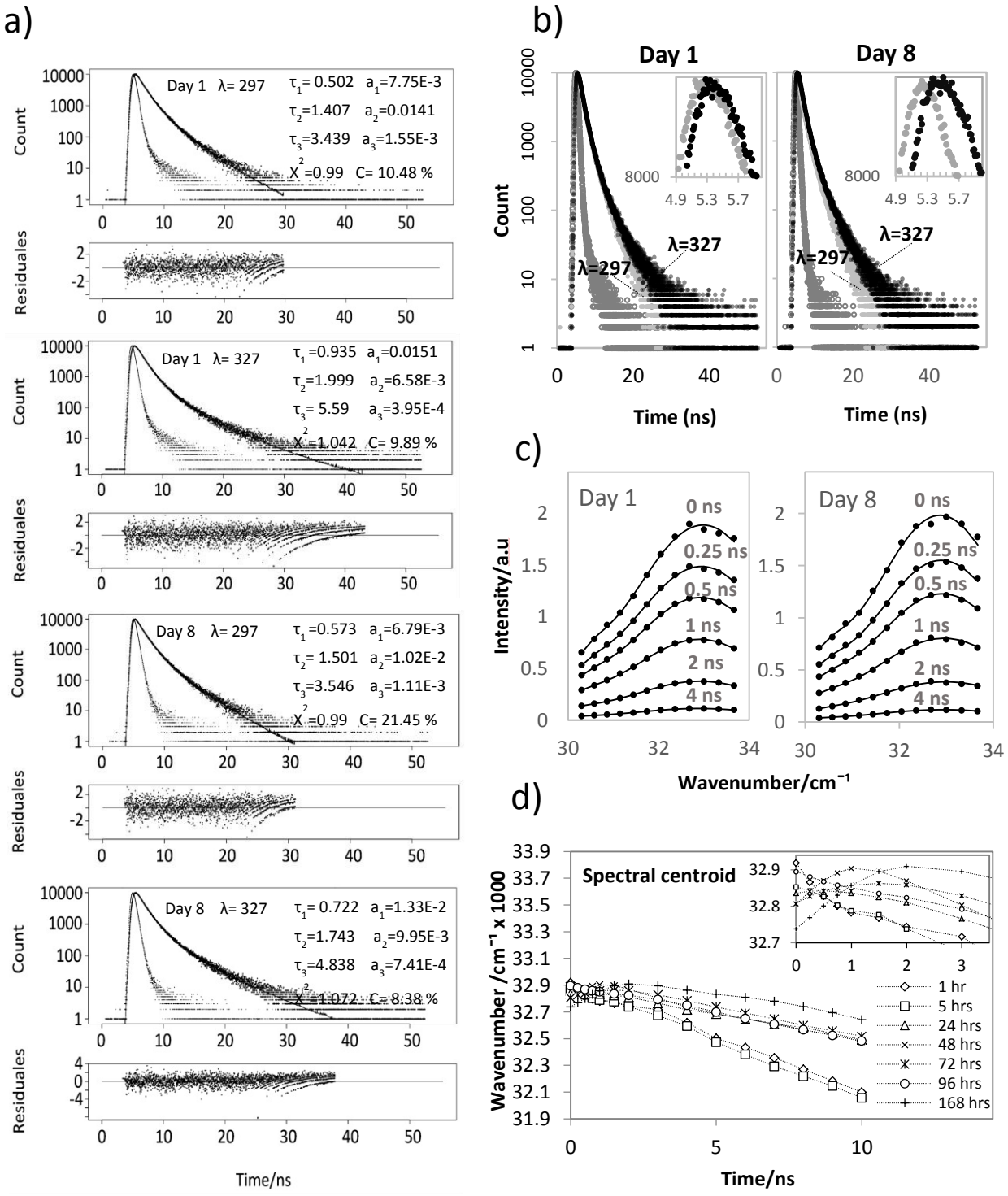
a)
Day 1 λ= 297
τ1= 0.502 a1=7.75E-3
τ2=1.407 a2=0.0141
τ3=3.439 a3=1.55E-3
X2=0.99 C= 10.48 %
Day 1 λ= 327
τ1=0.935 a1=0.0151
τ2=1.999 a2=6.58E-3
τ3= 5.59 a3=3.95E-4
X2=1.042 C= 9.89 %
Day 8 λ= 297
τ1=0.573 a1=6.79E-3
τ2= 1.501 a2=1.02E-2
τ3=3.546 a3=1.11E-3
X2=0.99 C= 21.45 %
Day 8 λ= 327
τ1= 0.722 a1=1.33E-2
τ2=1.743 a2=9.95E-3
τ3=4.838 a3=7.41E-4
X2=1.072 C= 8.38 %
Count
Residuales
Time/ns
b)
Day 1
Day 8
λ=297
λ=327
Count
Time (ns)
c)
Day 1
Day 8
0 ns
0.25 ns
0.5 ns
1 ns
2 ns
4 ns
Intensity/a.u
Wavenumber/cm⁻¹
d)
Spectral centroid
1 hr
5 hrs
24 hrs
48 hrs
72 hrs
96 hrs
168 hrs
Wavenumber /cm⁻¹ x 1000
Time/ns

a)

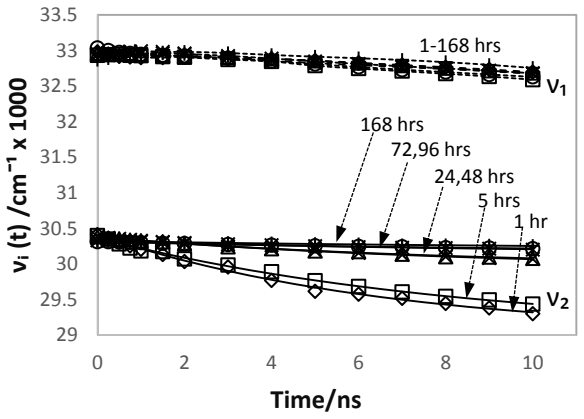
1-168 hrs
168 hrs
72,96 hrs
24,48 hrs
5 hrs
1 hr
ν_1
ν_2
ν_i (t) /cm^{-1} x 1000
Time/ns

b)

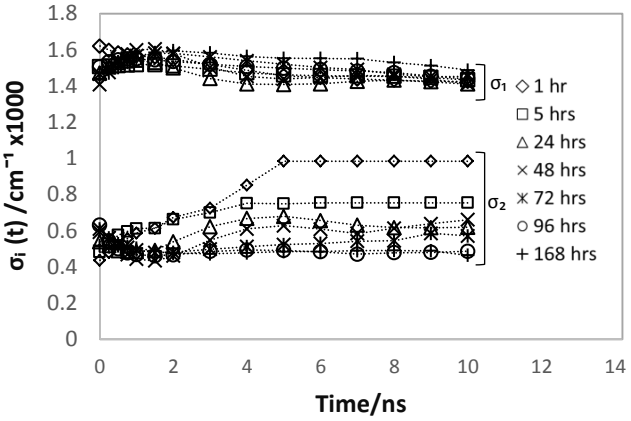
σ_1
σ_2
1 hr
5 hrs
24 hrs
48 hrs
72 hrs
96 hrs
168 hrs
σ_i (t) /cm^{-1} x1000
Time/ns

c)

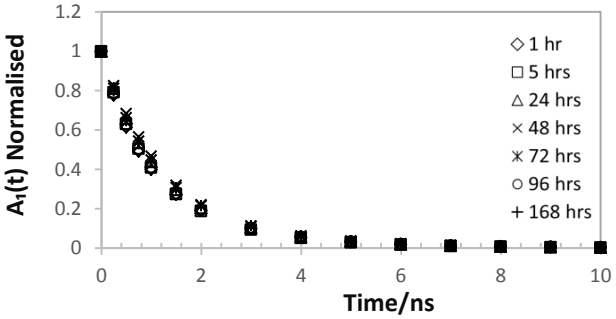
1 hr
5 hrs
24 hrs
48 hrs
72 hrs
96 hrs
168 hrs
A_1(t) Normalised
Time/ns

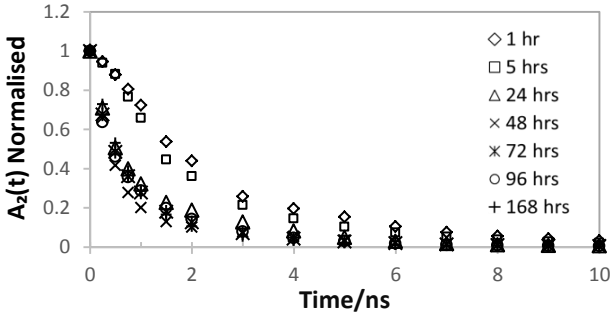
1 hr
5 hrs
24 hrs
48 hrs
72 hrs
96 hrs
168 hrs
A_2(t) Normalised
Time/ns

d)

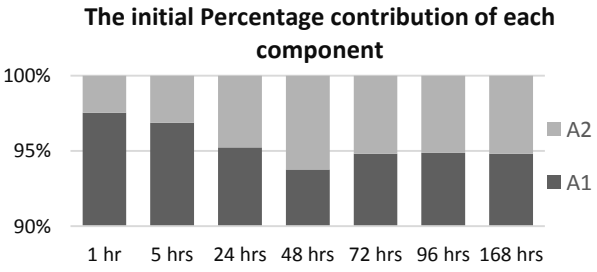
The initial Percentage contribution of each component
100%
95%
90%
A2
A1
1 hr
5 hrs
24 hrs
48 hrs
72 hrs
96 hrs
168 hrs

e)

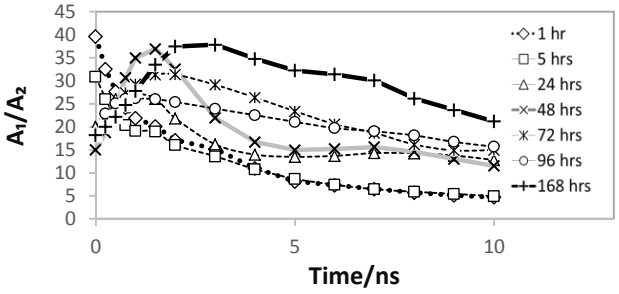
1 hr
5 hrs
24 hrs
48 hrs
72 hrs
96 hrs
168 hrs
A_1/A_2
Time/ns